

Bayesian inversion of azimuthal seismic amplitude data for indicators of interconnected aligned cracks

Huaizhen Chen* and Kristopher A. Innanen

ABSTRACT

Detection of natural fractures and identification of infilling fluids in fractures are important objectives in exploration and characterization of unconventional reservoirs (e.g. shale or tight sand reservoirs). In the case of rocks containing interconnected aligned fractures, both anisotropy and attenuation appears in reflected amplitudes of seismic wave. Starting with an effective model of interconnected aligned fractures in an elastic and isotropic background, we first present simplified complex stiffness parameters as a function of attenuation factor $1/Q$ in an attenuative anisotropic medium, and perturbations in stiffness parameters across an interface separating two attenuative anisotropic media. Using an approximate relationship between reflection coefficient and scattering potentials, we derive a linearized complex PP-wave reflection coefficient in terms of reflectivities of P- and S-wave moduli and density and changes in the tangential fracture weakness δ_T and attenuation factor $1/Q$, which provides a possibility to estimate fracture weakness and attenuation factor from reflection amplitudes. Based on the derived reflection coefficient, we propose an inversion approach of employing real and imaginary parts of complex seismic data in frequency domain for estimating unknown parameters following a Bayesian framework. Applying the inversion approach to frequency-dependent synthetic seismic datasets of different incidence and azimuthal angles, we may obtain the inverted tangential fracture weakness that can match the true value, and the attenuation factor can be estimated reliably even though the estimation should be improved at the location of fractured reservoir. Future work should focus on the illustration of stability and robustness of the proposed inversion approach and the verification of reliability of the approach using real datasets.

INTRODUCTION

Interconnected fractures are important pathways for fluid movements within rocks when seismic wave propagates in underground layers. Anisotropy and attenuation can be observed in reflected seismic amplitude, which behaves as amplitude variation with incidence and azimuthal angles (AVAZ) and change of seismic wave phase during seismic wave propagation; and estimating anisotropy and attenuation from seismic AVAZ data can provide information for the identification of hydrocarbon-bearing fractured reservoirs.

In the case of a rock containing interconnected aligned fractures, Hudson et al. (1996) present how fracture connectivity and infilling materials affect the displacement and propose stiffness parameters in terms of fluid and fracture properties (e.g. fluid bulk modulus, fracture density). Pointer et al. (2000) model the influence of fractures and fluids on seismic wave velocity and attenuation factor variation with frequency for two cases of a rock containing interconnected aligned cracks and that containing interconnected randomly oriented

*School of Ocean and Earth Science, Tongji University, Shanghai, China; and CREWES Project, University of Calgary, Calgary, Alberta, Canada. Email: huaizhen.chen@tongji.edu.cn

cracks. Rubino et al. (2017) conclude that fracture connectivity can reduce anisotropy, and Guo et al. (2018) present expressions of dynamic stiffness parameters and anisotropic parameters in the case of rocks containing interconnected two orthogonal fractures.

Features of frequency-dependent AVAZ data can provide valuable information for estimating where natural fractures exist and what types of infilling fluids are in fractures. Focusing on a rock containing a single set of parallel cracks, Chen et al. (2020) present an indicator of oil-bearing fractured reservoirs, in which a fluid movement related parameter is involved, and propose an inversion approach of employing real parts of frequency-dependent AVAZ data to estimate the indicator and fracture weaknesses; however, the imaginary part that is much sensitive to fluids has been ignored.

In the present study, starting with an effective model of a rock containing interconnected aligned fractures, we first present simplified complex stiffness parameters as a function of attenuation factor $1/Q$ in the case of infilling fluids being a mixture of water and oil, and the attenuation factor is involved in the imaginary parts. Using the simplified stiffness parameters, we derive a linearized PP-wave reflection coefficient in terms of perturbations in the tangential fracture weakness δ_T and the attenuation factor $1/Q$ across an interface separating two attenuative anisotropic media. Based on the derived reflection coefficient, we establish an approach of employing both real and imaginary parts of azimuthal AVAZ datasets to estimate fracture weakness and attenuation factor. We apply the inversion approach to frequency-dependent synthetic seismic data of different incidence and azimuthal angles, and we obtain the inversion results of fracture weakness and attenuation factor that may match true values. The future work should focus on the verification of stability and robustness of the inversion approach, and clarify how to apply the inversion approach to real datasets to provide valuable information for the detection of natural fractures and the identification of infilling fluids.

THEORY AND METHOD

In this section, we derive the complex reflection coefficient in terms of indicators of fluids and cracks in the case of an interface separating two attenuative anisotropic media; and we present an approach of employing real and imaginary parts of azimuthal seismic data variation with frequency and incidence angle (Frequency-dependent AVAZ) to estimate the tangential fracture weakness and attenuation factor.

Stiffness parameters of rocks containing interconnected aligned cracks

In the case of normals of cracks being aligned along x_1 -axis, the complex stiffness matrix of a cracked rock $\tilde{\mathbf{C}}$ is given by Hudson (1980) as

$$\tilde{\mathbf{C}} = \begin{bmatrix} \tilde{C}_{11} & \tilde{C}_{12} & \tilde{C}_{12} & 0 & 0 & 0 \\ \tilde{C}_{12} & \tilde{C}_{33} & \tilde{C}_{23} & 0 & 0 & 0 \\ \tilde{C}_{12} & \tilde{C}_{23} & \tilde{C}_{33} & 0 & 0 & 0 \\ 0 & 0 & 0 & \tilde{C}_{44} & 0 & 0 \\ 0 & 0 & 0 & 0 & \tilde{C}_{55} & 0 \\ 0 & 0 & 0 & 0 & 0 & \tilde{C}_{66} \end{bmatrix} \quad (1)$$

$$= \begin{bmatrix} M - \frac{M}{g} e \tilde{U}_{33} & \lambda - \frac{\lambda}{g} e \tilde{U}_{33} & \lambda - \frac{\lambda}{g} e \tilde{U}_{33} & 0 & 0 & 0 \\ \lambda - \frac{\lambda}{g} e \tilde{U}_{33} & M - M \frac{(1-2g)^2}{g} e \tilde{U}_{33} & \lambda - \lambda \frac{1-2g}{g} e \tilde{U}_{33} & 0 & 0 & 0 \\ \lambda - \frac{\lambda}{g} e \tilde{U}_{33} & \lambda - \lambda \frac{1-2g}{g} e \tilde{U}_{33} & M - M \frac{(1-2g)^2}{g} e \tilde{U}_{33} & 0 & 0 & 0 \\ 0 & 0 & 0 & \mu & 0 & 0 \\ 0 & 0 & 0 & 0 & \mu - \mu e \tilde{U}_{11} & 0 \\ 0 & 0 & 0 & 0 & 0 & \mu - \mu e \tilde{U}_{11} \end{bmatrix},$$

where $g = \mu/M$, $M = \lambda + 2\mu$, λ and μ are Lamé parameters of the isotropic background rock, e is crack density, and \tilde{U}_{11} and \tilde{U}_{33} are variables influenced by crack properties (e.g. crack aspect ratio) and fluid parameters (e.g. fluid bulk modulus). In the case of interconnected aligned cracks embedding in an isotropic background rock, \tilde{U}_{11} and \tilde{U}_{33} are expressed as (Pointer et al., 2000)

$$\tilde{U}_{11} = \frac{16}{3} \frac{1}{3-2g} \frac{1}{1 + \frac{4}{\pi\alpha} \frac{i\omega\eta_f}{\mu} \frac{1}{3-2g}},$$

$$\tilde{U}_{33} = \frac{4}{3} \frac{1}{1-g} \left(1 - \frac{\Gamma}{1 - i\omega\tau} \right), \quad (2)$$

where ω is the angular frequency, and

$$\Gamma = \frac{\left(\frac{K_f}{\pi\mu\alpha} \frac{1}{1-g} \right)}{1 + \left(\frac{K_f}{\pi\mu\alpha} \frac{1}{1-g} \right)},$$

$$\tau = \frac{3}{4\pi} \frac{K_f}{\eta_f} \frac{P_e}{e\alpha} \frac{1}{V^2}, \quad (3)$$

in which η_f is fluid viscosity, α is crack aspect ratio, K_f is fluid bulk modulus, P_e is permeability of cracked rock, and V is wave speed.

Pointer et al. (2000) point out only in the case of $\alpha \leq 10^{-5}$ and $f \geq 100\text{kHz}$, \tilde{U}_{11} generates a significant attenuation, which is outside the realm of seismology. Hence, focusing on the seismic frequency range, we neglect the attenuation generated by \tilde{U}_{11} , and we expand and rewrite \tilde{U}_{33} as

$$\tilde{U}_{33} \approx \frac{4}{3} \frac{1}{1-g} (1 - \Gamma - i\omega\Gamma\tau). \quad (4)$$

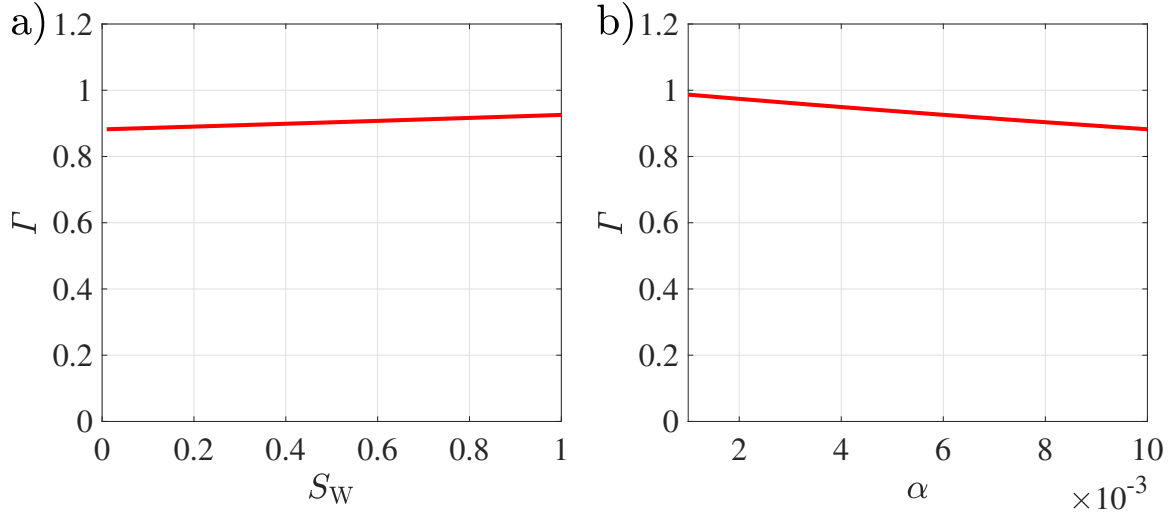


FIG. 1. a) Variation of Γ with water saturation S_W in the case of $\alpha = 0.01$; b) Variation of Γ with crack aspect ratio α in the case of $S_W = 0.5$. Bulk moduli of water and oil are 2.25 GPa and 1.35 GPa, respectively; $g = 0.36$ and $\mu = 9$ GPa are used as elastic parameters of the isotropic background rock.

Focusing on oil-bearing fractures, we show how Γ varies with water saturation S_W and crack aspect ratio α in the case that fluids in cracks are the mixture of oil and water, as plotted in Figure 1. We observe the value of Γ varies in the range 0.8 – 1 for oil-bearing cracked reservoirs in the case of $\alpha \leq 0.01$, and we may use $\Gamma \approx 1$ to further simplify \tilde{U}_{33} . Hence, in this study, the simplified and approximate expressions of U_{11} and U_{33} are given by

$$\begin{aligned}\tilde{U}_{11} &\approx \frac{16}{3} \frac{1}{3 - 2g}, \\ \tilde{U}_{33} &\approx \frac{4}{3} \frac{1}{1 - g} (-i\omega\tau).\end{aligned}\quad (5)$$

Substituting equation 5 into equation 1, we obtain the approximate and simplified stiffness parameters as

$$\begin{aligned}\tilde{C}_{11} &\approx M \left(1 + \omega \frac{i}{Q} \right), \\ \tilde{C}_{12} &\approx \lambda \left(1 + \omega \frac{i}{Q} \right), \\ \tilde{C}_{22} &\approx M \left[1 + (1 - 2g)^2 \omega \frac{i}{Q} \right], \\ \tilde{C}_{23} &\approx \lambda \left[1 + (1 - 2g) \omega \frac{i}{Q} \right], \\ C_{55} &\approx \mu - \mu \delta_{\Gamma},\end{aligned}\quad (6)$$

where $1/Q$ and δ_T are attenuation factor and tangential fracture weakness given by

$$\frac{1}{Q} = \frac{1}{\pi} \frac{P_e K_f}{\alpha \eta_f} \frac{1}{g(1-g)} \frac{1}{V^2},$$

$$\delta_T = \frac{16e}{3(3-2g)}. \quad (7)$$

In equation 7, we observe that the tangential fracture weakness δ_T is mainly affected by fracture density, which means δ_T may be used an indicator of cracks. For oil-bearing fractured reservoirs, we model how the attenuation factor $1/Q$ varies with fracture density e , water saturation S_W and fracture aspect ratio α , as displayed in Figure 2. In Appendix A, we show how to compute the total permeability P_e , fluid bulk modulus K_f , and fluid viscosity η_f using fracture parameters (e.g. fracture density and aspect ratio) and fluid content (e.g. water saturation).

In Figures 2a and 2b, we observe that the attenuation factor increases with water saturation S_W and hardly changes with the fracture aspect ratio α , and $1/Q$ shows a relatively low value in the case of oil-bearing reservoir. However, in Figure 2c, we see that the attenuation factor changes much more faster with fracture density e than it changes with water saturation S_W .

Since $1/Q$ is influenced by both fracture density and fluid saturation, we should establish a more sensitive fluid indicator, e.g. a novel factor combining $1/Q$ and δ_T , in which we try to remove the effect of fracture density using the tangential fracture weakness. In this study, we will implement the inversion for the attenuation factor $1/Q$ and the tangential fracture weakness δ_T , and then we combine the inversion results of $1/Q$ and δ_T to identify the oil-bearing fractured reservoirs.

Derivation of linearized reflection coefficient in attenuative anisotropic media

Using the simplified stiffness parameters shown in equation 7, we first express perturbations in stiffness parameters across a reflection interface separating two attenuative anisotropic media as shown in Figure 3.

In the case that changes in elastic properties (i.e. ΔM , $\Delta\lambda$, and μ) across the reflection interface and the attenuation factor of the background rock are small, we express the perturbations in stiffness parameters as

$$\Delta\tilde{C}_{11} \approx \Delta M + i\omega M \Delta \frac{1}{Q},$$

$$\Delta\tilde{C}_{12} \approx \Delta\lambda + i\omega\lambda \Delta \frac{1}{Q},$$

$$\Delta\tilde{C}_{22} \approx \Delta M + i\omega M(1-2g)^2 \Delta \frac{1}{Q},$$

$$\Delta\tilde{C}_{23} \approx \Delta\lambda + i\omega\lambda(1-2g) \Delta \frac{1}{Q},$$

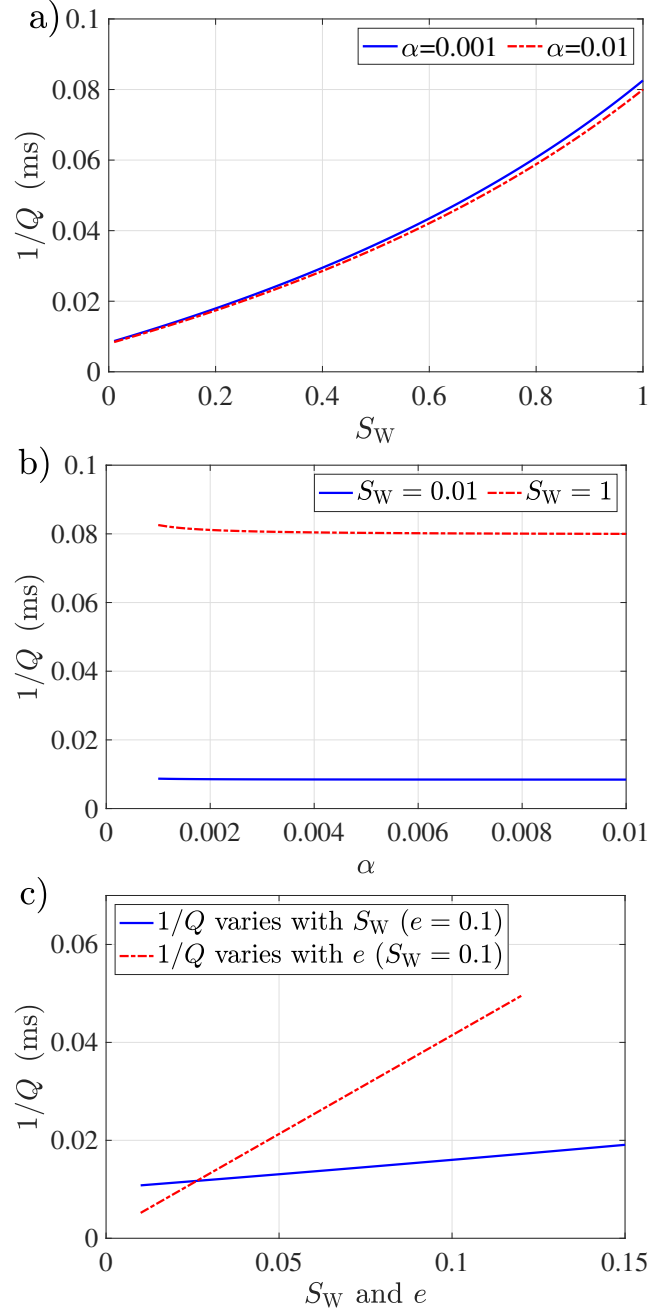


FIG. 2. a) Variation of attenuation factor with water saturation S_W ; and b) Variation of attenuation factor with fracture aspect ratio. Parameters used for computing $1/Q$ are $V = 3300$ m/s and $g = 0.36$. Fracture aperture is $h = 0.0001$ m

$$\Delta C_{44} = \Delta\mu,$$

$$\Delta C_{55} \approx \Delta\mu - \mu\Delta\delta_T, \quad (8)$$

where $\Delta\frac{1}{Q}$ and $\Delta\delta_T$ are perturbations in attenuation factor and tangential weakness across the reflection interface, respectively. We emphasize that we neglect the term that is proportional to $\frac{1}{Q}\Delta M$, $\Delta M\Delta\frac{1}{Q}$, $\delta_T\Delta\mu$, and $\Delta\mu\Delta\delta_T$ in the derivation of perturbations in stiffness parameters. We employ the scattering potential given by Beylkin and Burridge (1990) and Shaw and Sen (2006) to derive a P-to-P reflection coefficient for the interface separating

$M - \frac{1}{2}\Delta M, \quad \mu - \frac{1}{2}\Delta\mu, \quad \rho - \frac{1}{2}\Delta\rho,$ $Q^{-1} - \frac{1}{2}\Delta Q^{-1}, \quad \delta_T - \frac{1}{2}\Delta\delta_T$
Interface
$M + \frac{1}{2}\Delta M, \quad \mu + \frac{1}{2}\Delta\mu, \quad \rho + \frac{1}{2}\Delta\rho,$ $Q^{-1} + \frac{1}{2}\Delta Q^{-1}, \quad \delta_T + \frac{1}{2}\Delta\delta_T$

FIG. 3. A reflection interface separating two attenuative media. Parameters M , μ , ρ , δ_T , and Q^{-1} are P- and S-wave moduli, density, tangential fracture weakness, and attenuation factor of background medium, and ΔM , $\Delta\mu$, $\Delta\rho$, $\Delta\delta_T$, and ΔQ^{-1} are the corresponding perturbations.

two attenuative anisotropic media as

$$R_{PP} = \frac{\Delta\rho \cos 2\theta}{4\rho \cos^2 \theta} + \frac{1}{4\rho \cos^2 \theta} \left(\begin{array}{l} +\Delta C_{11} \frac{\rho \sin^4 \theta \cos^4 \phi}{M} \\ +\Delta C_{12} \left(\frac{2\rho \sin^4 \theta \cos^2 \phi \sin^2 \phi}{M} + \frac{2\rho \sin^2 \theta \cos^2 \theta \cos^2 \phi}{M} \right) \\ +\Delta C_{23} \frac{2\rho \sin^2 \theta \cos^2 \theta \sin^2 \phi}{M} \\ +\Delta C_{33} \left(\frac{\rho \sin^4 \theta \sin^4 \phi}{M} + \frac{\rho \cos^4 \theta}{M} \right) \\ +\Delta C_{44} \left(\frac{-4\rho \sin^2 \theta \cos^2 \theta \sin^2 \phi}{M} \right) \\ +\Delta C_{55} \left(\frac{4\rho \sin^4 \theta \cos^2 \phi \sin^2 \phi}{M} - \frac{4\rho \sin^2 \theta \cos^2 \theta \cos^2 \phi}{M} \right) \end{array} \right), \quad (9)$$

where θ is the incidence angle of P wave, and ϕ is azimuth indicating difference between the symmetry of cracks (i.e. x_1 -axis) and the source-receiver seismic line. Combining equations 8 and 9, we derive the P-to-P reflection coefficient after some algebra as

$$R_{PP}(\theta, \phi, \omega) = \mathcal{R} + i \mathcal{Q}, \quad (10)$$

where

$$\begin{aligned} \mathcal{R} &= \frac{1}{4\cos^2 \theta} R_M - 2g \sin^2 \theta R_\mu + \frac{\cos 2\theta}{4\cos^2 \theta} R_\rho \\ &\quad + g \sin^2 \theta \cos^2 \phi (1 - \tan^2 \theta \sin^2 \theta) R_T, \\ \mathcal{Q} &= \frac{\omega}{4\cos^2 \theta} [1 - 2g (\sin^2 \theta \sin^2 \phi + \cos^2 \theta)]^2 R_Q, \end{aligned} \quad (11)$$

and where $R_M = \Delta M/M$, $R_\mu = \Delta\mu/\mu$ and $R_\rho = \Delta\rho/\rho$ are reflectivities of P- and S-wave moduli and density of the isotropic elastic background rock, $R_T = \Delta\delta_T$, and $R_Q = \Delta(1/Q)$. In the derived linearized P-to-P reflection coefficient, we observe the attenuation factor only appears in the imaginary part, and the variation of real part with azimuth ϕ is only related to the tangential fracture weakness. Hence, in the present study, we focus on proposing an inversion approach of employing seismic reflection amplitude variation with incidence angle, azimuth and frequency (AVAZF) to estimate the tangential fracture weakness δ_T and the attenuation factor $\frac{1}{Q}$.

Inversion for attenuation factor and tangential fracture weakness

The convolutional model for generating seismic data of different incidence and azimuthal angles is expressed in frequency domain as

$$S(\theta, \phi, \omega) = W(\omega) R_{PP}(\theta, \phi, \omega), \quad (12)$$

where $S = X + iY$ and $W = A + iB$ are seismic and wavelet in frequency domain, respectively. In the case of seismic data of two azimuths ϕ_1 and ϕ_2 , the difference between the seismic data in the frequency domain is expressed as

$$\Delta S(\theta, \phi_1, \phi_2, \omega) = W(\omega) \Delta R_{PP}(\theta, \phi_1, \phi_2, \omega), \quad (13)$$

where $\Delta R_{PP}(\theta, \phi_1, \phi_2, \omega)$ is the difference between reflection coefficients of ϕ_1 and ϕ_2 in the frequency domain. Combining equations 10 and 13, we express differences between seismic data of ϕ_1 and ϕ_2 as

$$\begin{bmatrix} \Delta X(\theta, \phi_1, \phi_2, \omega) \\ \Delta Y(\theta, \phi_1, \phi_2, \omega) \end{bmatrix} = \begin{bmatrix} A p_T & -B p_Q \\ B p_T & A p_Q \end{bmatrix} \begin{bmatrix} R_T \\ R_Q \end{bmatrix}, \quad (14)$$

where

$$\begin{aligned} p_T &= g \sin^2 \theta (\cos^2 \phi_2 - \cos^2 \phi_1) (1 - \tan^2 \theta \sin^2 \theta), \\ p_Q &= g \omega \tan^2 \theta (\sin^2 \phi_2 - \sin^2 \phi_1) [1 - g \sin^2 \theta (\sin^2 \phi_2 + \sin^2 \phi_1) - 2g \cos^2 \theta]. \end{aligned} \quad (15)$$

Equation 14 can be expressed succinctly as

$$\mathbf{d} = \mathbf{Gm}, \quad (16)$$

where \mathbf{d} is vector of input data involving differences in real and imaginary parts computed using seismic data of ϕ_1 and ϕ_2 in frequency domain, \mathbf{G} is the operator related to the frequency, incidence and azimuthal angles, and \mathbf{m} is the model vector involving reflectivities of tangential fracture weakness $\Delta \delta_T$ and attenuation factor $\Delta \frac{1}{Q}$, respectively.

Following a Bayesian framework, we implement the inversion of azimuthal amplitude difference variation with frequency and incidence for estimating the unknown parameter vector using probabilistic constraints. The posterior Probability Distribution Function (PDF), $P(\mathbf{m}|\mathbf{d})$, is computed using the likelihood function, $P(\mathbf{d}|\mathbf{m})$, and a prior PDF, $P(\mathbf{m})$, as

$$P(\mathbf{m}|\mathbf{d}) \approx P(\mathbf{d}|\mathbf{m}) P(\mathbf{m}), \quad (17)$$

and in the case of the noise being assumed to be Gaussian, we write the likelihood function as

$$P(\mathbf{d}|\mathbf{m}) \propto \exp\left(-\frac{(\mathbf{d} - \mathbf{Gm})^\dagger (\mathbf{d} - \mathbf{Gm})}{2\sigma_n^2}\right), \quad (18)$$

where \dagger denotes the transpose, and σ_n^2 is the variance of the noise. To produce a sparse solution for the unknown parameter vector, we employ the univariate Cauchy distribution priori to constrain the inversion problem, and in the case of N interface, the expression of $P(\mathbf{m})$ is given by

$$P(\mathbf{m}) \propto \exp\left(-\sum_{l=1}^{2N} \ln\left(1 + \left(\frac{m_l}{\sigma_m}\right)^2\right)\right), \quad (19)$$

where σ_m is a scale value that is related to the variance of the unknown parameter vector. Hence, we obtain the posterior PDF as

$$P(\mathbf{m}|\mathbf{d}) \approx \exp\left(-\frac{(\mathbf{d} - \mathbf{G}\mathbf{m})^\dagger (\mathbf{d} - \mathbf{G}\mathbf{m})}{2\sigma_n^2} - \sum_{l=1}^{2N} \ln\left(1 + \left(\frac{m_l}{\sigma_m}\right)^2\right)\right). \quad (20)$$

To implement the inversion for the unknown parameter vector, we need to minimize the following objective function

$$J(\mathbf{m}) = \frac{(\mathbf{d} - \mathbf{G}\mathbf{m})^\dagger (\mathbf{d} - \mathbf{G}\mathbf{m})}{2\sigma_n^2} + \sum_{l=1}^{2N} \ln\left(1 + \left(\frac{m_l}{\sigma_m}\right)^2\right), \quad (21)$$

to obtain the maximum posterior PDF. We compute the derivative of $J(\mathbf{m})$ with respect to \mathbf{m} as

$$\frac{\partial J(\mathbf{m})}{\partial \mathbf{m}} = \frac{-\mathbf{d}^\dagger \mathbf{G} + \mathbf{m}^\dagger \mathbf{G}^\dagger \mathbf{G}}{\sigma_n^2} + \frac{2}{\sigma_m^2} \mathbf{U} \mathbf{m}, \quad (22)$$

where $\mathbf{U}_{ll} = 1 + \left(\frac{m_l}{\sigma_m}\right)^2$ is a diagonal matrix, and letting the derivative of $J(\mathbf{m})$ with respect to \mathbf{m} be zero, we get

$$\mathbf{m} = \left(\mathbf{G}^\dagger \mathbf{G} + \frac{2\sigma_n^2}{\sigma_m^2} \mathbf{U}\right)^{-1} \mathbf{G}^\dagger \mathbf{d}. \quad (23)$$

In equation 22, we observe the matrix \mathbf{U}_{ll} is related to the unknown parameter itself, which means the inversion for \mathbf{m} is a nonlinear problem; hence, following Alemie (2010), we employ the Iterative re-weighted least squares (IRLS) method to obtain the final inversion results of δ_T and $\frac{1}{Q}$.

NUMERICAL EXAMPLES

In this section, we first model how real and imaginary parts of reflection coefficient variation with incidence angle and azimuth in the case of different values of frequency, and then we generate synthetic complex seismic data in frequency and utilize real and imaginary parts of synthetic data to implement the inversion for indicators of fractures and fluids.

Frequency-dependent reflection amplitude variation with incidence angle and azimuth (Frequency-dependent AVAZ)

Given an interface separating two attenuative anisotropic layers, we model how the frequency-dependent reflection coefficient varies with incidence and azimuthal angles. Table 1 shows P- and S-wave moduli (M and μ), density (ρ), tangential fracture weakness (δ_T) and attenuation factor ($1/Q$) of two attenuative anisotropic layers, and we assume the lower layer shows relatively high values of fracture weakness and attenuation factor. We calculate the complex reflection coefficients using the derived equation 11, and we plot the real and imaginary parts of reflection coefficients varying with incidence and azimuthal angles in Figure 4.

Table 1. Parameters of sand-shale model

	M (GPa)	μ (GPa)	ρ (g/cm ³)	δ_T	$1/Q$
Upper layer	25	8.3	2.3	0.01	0.01
Lower layer	12.5	3.38	2	0.35	0.5

Combining the derived reflection coefficient and the AVAZ modelling results, we observe both the real and imaginary parts of reflection coefficient vary with incidence and azimuthal angles; however, only the imaginary part of reflection coefficient changes with frequency.

Synthetic examples

We next apply the established inversion approach to synthetic datasets generated using a well-log model. In Figure 5a, we show curves of P- and S-wave velocities V_P and V_S and density ρ , and in Figure 5b, we plot crack porosity φ_{crack} , water saturation S_W and the computed attenuation factor $\frac{1}{Q}$, tangential fracture weakness δ_T and a new parameter $\frac{1}{Q\delta_T}$.

In Figure 5, we plot the curve of oil-bearing reservoir in red. We observe at the location of oil-bearing reservoir, P- and S-wave velocities, density and water saturation show relatively low values, and the crack porosity shows relatively high values. However, the computed attenuation factor $\frac{1}{Q}$ exhibits relatively low values, which again verifies the attenuation factor is much more influenced by crack density than by fluid content. Hence, to identify fluid type in the fractured reservoirs, we establish a new indicator that combines $\frac{1}{Q}$ and δ_T , i.e. $\frac{1}{Q\delta_T}$, in which we try to get rid of the influence of fracture density via dividing $\frac{1}{Q}$ by δ_T . In the calculated result of $\frac{1}{Q\delta_T}$ shown in Figure 5b), we also observe at the location of oil-bearing reservoir the computed $\frac{1}{Q\delta_T}$ shows relatively low values, and the reason is the low water saturation S_W may produce a low fluid bulk modulus K_f and a high viscosity η_f , which finally induce a much lower value of $\frac{K_f}{\eta_f}$ in the attenuation factor $\frac{1}{Q}$.

Using the derived reflection coefficients, we first generate both real and imaginary parts

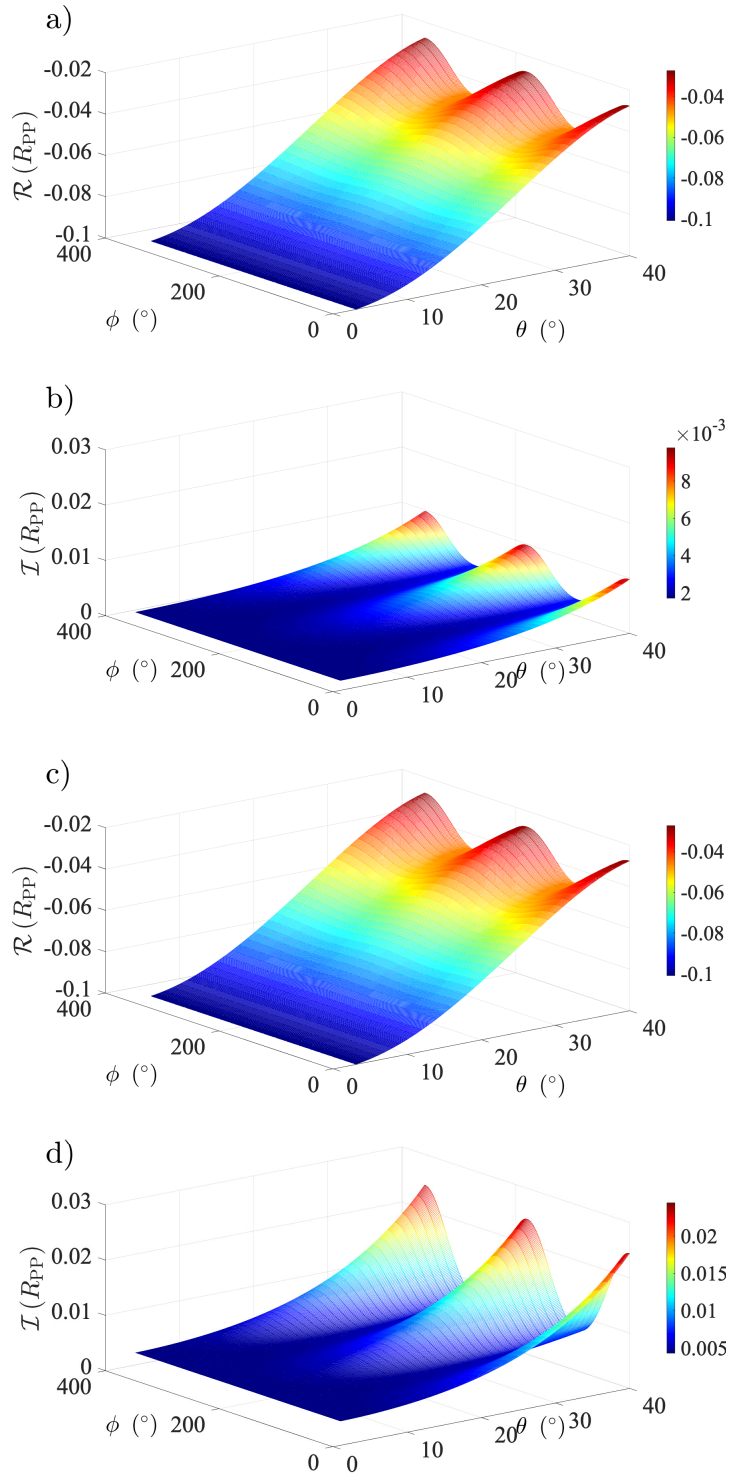


FIG. 4. Variation of complex reflection coefficients with incidence and azimuthal angles (AVAZ). a) and b) Real and imaginary parts of reflection coefficients of frequency 20 Hz; and c) and d) Real and imaginary parts of reflection coefficient of frequency 50 Hz.

of seismic data of different incidence angles ($\theta_1 = 10^\circ$, $\theta_2 = 20^\circ$ and $\theta_3 = 30^\circ$), azimuthal angles ($\phi_1 = 0^\circ$, $\phi_2 = 30^\circ$, and $\phi_3 = 60^\circ$) and frequencies ($f_1 = 10$ Hz and $f_2 = 30$ Hz)

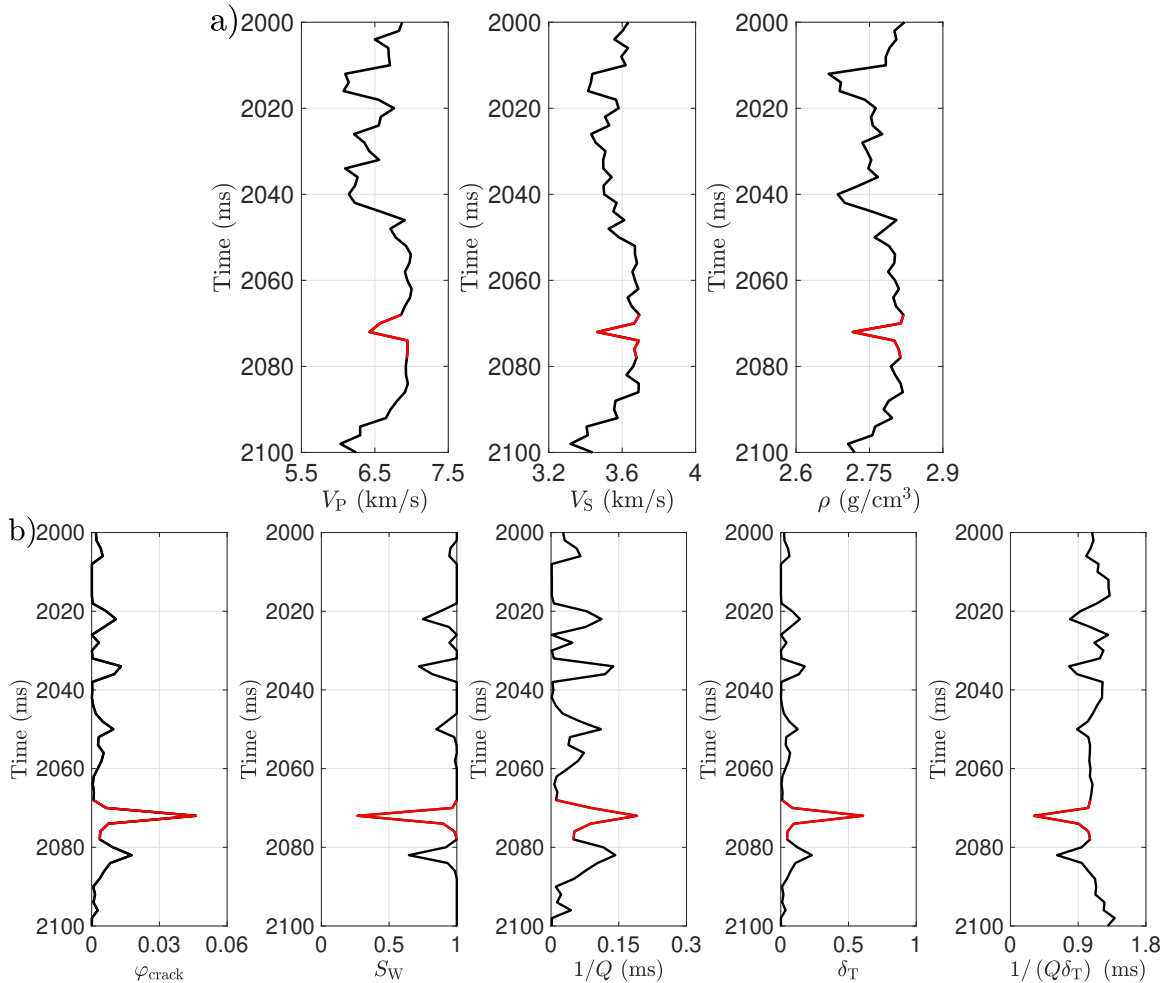


FIG. 5. a) Curves of P- and S-wave velocities V_P and V_S , density ρ ; b) Curves of crack porosity φ , water saturation S_W , the computed attenuation factor $1/Q$, the computed tangential fracture weakness δ_T and a new parameter combining $1/Q$ and δ_T . The curves plotted in red indicate an oil-bearing reservoir.

using a Ricker wavelet of dominant frequency 20 Hz, as shown in Figure 6. We observe that the difference between real parts of synthetic seismic data of frequency $f_1 = 10$ Hz and $f_2 = 30$ Hz is small, and the large difference exhibits in the imaginary parts of synthetic seismic data. At the location of fractured reservoir around time 2072 ms, we see the amplitude variation with the incidence angle exists. Employing the data of amplitude real and imaginary parts variation with frequency, incidence and azimuthal angles, we may implement the inversion for the tangential fracture weakness and attenuation factor, as shown in Figure 7. We observe there is a good match between the inversion result and the true value of tangential fracture weakness δ_T ; however, the inverted attenuation factor can match the true value except the area of fractured reservoir. We conclude the accuracy of inversion for attenuation factor should be improved by employing more frequency components of real and imaginary parts of seismic data.

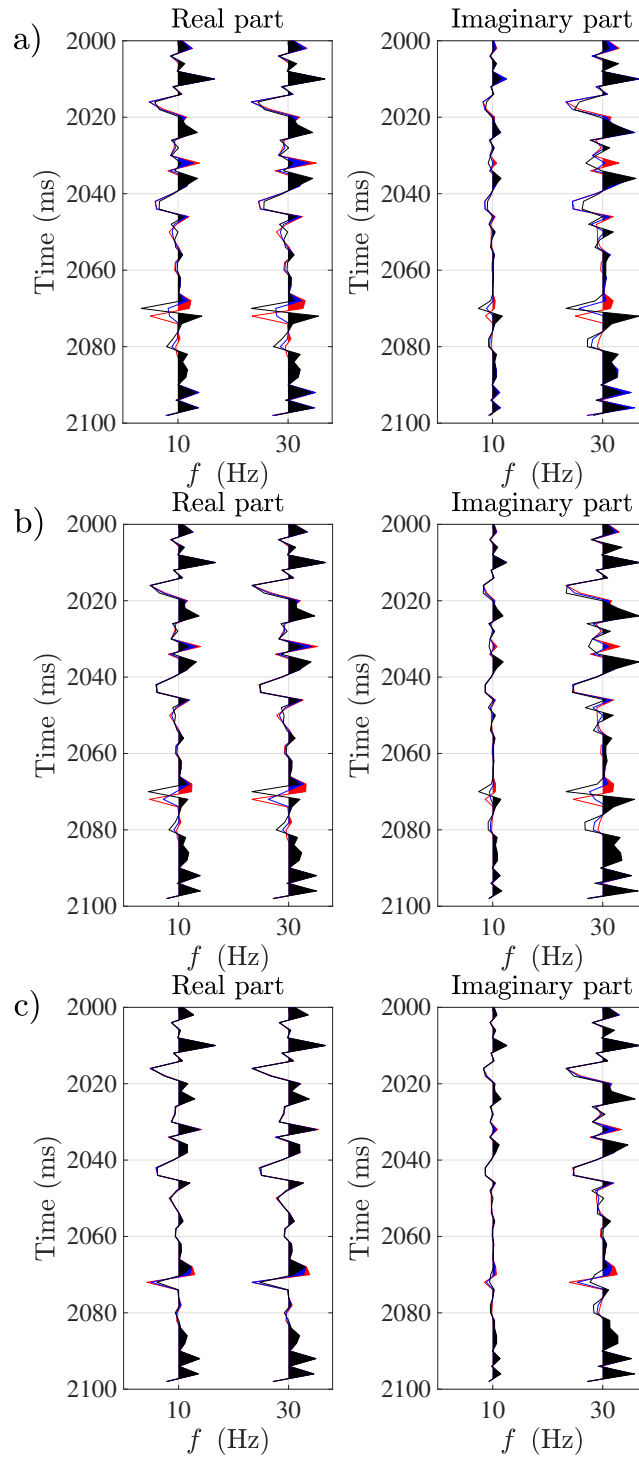


FIG. 6. Real and imaginary parts of synthetic seismic profiles of frequency $f_1 = 10$ Hz and $f_2 = 30$ Hz. a) $\phi_1 = 0^\circ$, b) $\phi_2 = 30^\circ$, and c) $\phi_3 = 60^\circ$. Seismic profiles plotted in red, blue and black represent the synthetic data generated for the case of incidence angle $\theta_1 = 10^\circ$, $\theta_2 = 20^\circ$ and $\theta_3 = 30^\circ$, respectively.

CONCLUSIONS

In the case of a rock containing interconnected aligned fractures, seismic wave propagation exhibits energy loss and anisotropy. Based on an effective model for intercon-

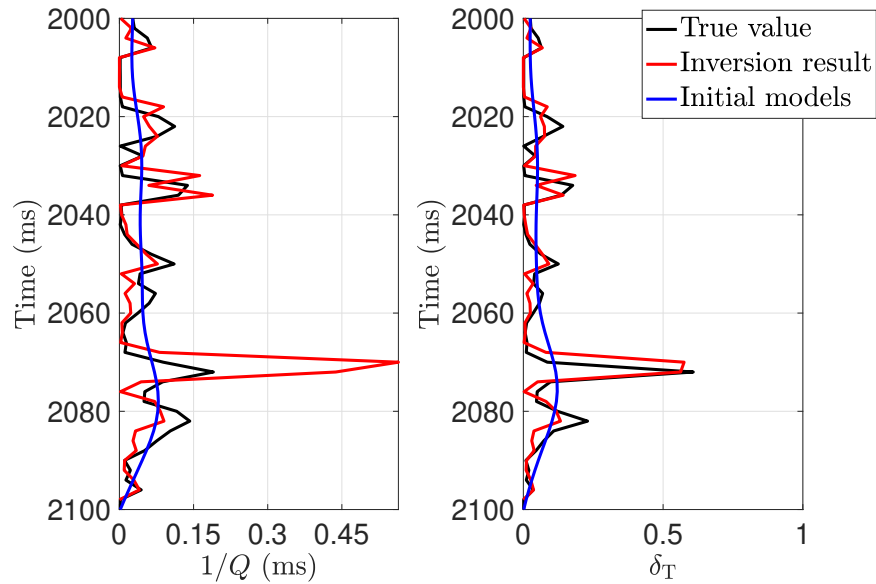


FIG. 7. Comparisons between inversion results and real values of tangential fracture weakness and attenuation factor. Initial model is the smoothed version of true value.

nected aligned fractures in an elastic and isotropic background, we first express simplified stiffness parameters in terms of elastic parameters (P- and S-wave moduli M and μ) and attenuation factor $\frac{1}{Q}$, and the attenuation factor is involved in the imaginary part of complex stiffness parameter. Using the simplified complex stiffness parameters, we express perturbations in stiffness parameters across an reflection interface separating two attenuative anisotropic media and derive a linearized complex PP-wave reflection coefficient in terms of reflectivities in elastic parameters and changes in attenuation factor and tangential fracture weakness, which is frequency-dependent and varies with incidence and azimuthal angles (Frequency-dependent AVAZ). Using the derived reflection coefficient, we propose an inversion approach of employing differences in frequency-dependent AVAZ data to estimate fracture weakness and attenuation factor following a Bayesian framework. We apply the proposed inversion approach to synthetic seismic datasets, and we employ the difference in real and imaginary parts of synthetic azimuthal complex seismic data of two different frequencies to estimate tangential fracture weakness and attenuation factor. We conclude that the tangential fracture weakness can be estimated reliably; however, the accuracy of the inversion for attenuation factor should be improved by involving AVAZ of more frequencies.

ACKNOWLEDGMENTS

The research was supported by the Fundamental Research Funds for the Central Universities. We thank the sponsors of CREWES for continued support. This work was funded by CREWES industrial sponsors, NSERC (Natural Science and Engineering Research Council of Canada) through the grants CRDPJ 461179-13 and CRDPJ 543578-19. Research Institute of Petroleum Exploration and Development-Northwest, Petrochina, is thanked for well log data.

APPENDIX A. EXPRESSIONS OF ROCK PERMEABILITY AND FLUID BULK MODULUS AND VISCOSITY

For the case of fractured rocks with a tight background (i.e. the permeability of tight background $P_e \approx 0$), the total permeability of the fractured rock is computed as (Mavko et al., 2009)

$$P_e \approx \frac{h^2}{12} \varphi_{\text{crack}}, \quad (\text{A.1})$$

where h is fracture aperture, and φ is fracture porosity expressed as

$$\varphi_{\text{crack}} = \frac{4}{3} \pi e \alpha, \quad (\text{A.2})$$

where the fracture aspect ratio α is computed as

$$\alpha = \frac{h}{l}, \quad (\text{A.3})$$

in which l is the semimajor axis of fracture.

In the case of fluids being the mixture of water and oil, the bulk modulus and viscosity of the fluids are given by

$$\begin{aligned} \frac{1}{K_f} &= \frac{1}{K_W} + \frac{1}{K_O}, \\ \frac{1}{\eta_f} &= \frac{1}{\eta_W} + \frac{1}{\eta_O}, \end{aligned} \quad (\text{A.4})$$

where K_W and K_O are bulk moduli of water and oil, and η_W and η_O are the viscosity of water and oil.

REFERENCES

- Alemie, W. M., 2010, Regularization of the AVO inverse problem by means of a multivariate Cauchy probability distribution: M.Sc. thesis, University of Alberta.
- Beylkin, G., and Burridge, R., 1990, Linearized inverse scattering problems in acoustics and elasticity: *Wave motion*, **12**, No. 1, 15–52.
- Chen, H., Li, J., and Innanen, K. A., 2020, Inversion of differences in frequency components of azimuthal seismic data for indicators of oil-bearing fractured reservoirs based on an attenuative cracked model: *Geophysics*, **85**, No. 3, R163–R175.
- Guo, J., Rubino, J. G., Glubokovskikh, S., and Gurevich, B., 2018, Dynamic seismic signatures of saturated porous rocks containing two orthogonal sets of fractures: Theory versus numerical simulations: *Geophysical Journal International*, **213**, No. 2, 1244–1262.
- Hudson, J., 1980, Overall properties of a cracked solid: *Mathematical Proceedings of the Cambridge Philosophical Society*, **88**, No. 2, 371–384.
- Hudson, J., Liu, E., and Crampin, S., 1996, The mechanical properties of materials with interconnected cracks and pores: *Geophysical Journal International*, **124**, No. 1, 105–112.
- Mavko, G., Mukerji, T., and Dvorkin, J., 2009, *The rock physics handbook: Tools for seismic analysis of porous media*: Cambridge university press.
- Pointer, T., Liu, E., and Hudson, J. A., 2000, Seismic wave propagation in cracked porous media: *Geophysical Journal International*, **142**, No. 1, 199–231.
- Rubino, J., Caspari, E., Müller, T. M., and Holliger, K., 2017, Fracture connectivity can reduce the velocity anisotropy of seismic waves: *Geophysical Journal International*, **210**, No. 1, 223–227.
- Shaw, R. K., and Sen, M. K., 2006, Use of AVOA data to estimate fluid indicator in a vertically fractured medium: *Geophysics*, **71**, No. 3, C15–C24.